

1 **Association of *CXCR6* with COVID-19 severity: Delineating the host genetic factors in**
2 **transcriptomic regulation**

3 Yulin Dai^{1†}, Junke Wang^{2†}, Hyun-Hwan Jeong¹, Wenhao Chen^{3,4}, Peilin Jia¹, Zhongming
4 Zhao^{1,2,5*}

5 ¹Center for Precision Health, School of Biomedical Informatics, The University of Texas Health
6 Science Center at Houston, Houston, TX 77030, USA

7 ²MD Anderson Cancer Center UTHHealth Graduate School of Biomedical Sciences, Houston, TX,
8 USA

9 ³Immunobiology and Transplant Science Center, Department of Surgery, Houston Methodist
10 Research Institute and Institute for Academic Medicine, Houston Methodist Hospital, Houston,
11 TX 77030, USA

12 ⁴Department of Surgery, Weill Cornell Medicine, Cornell University, New York, NY 10065,
13 USA

14 ⁵Human Genetics Center, School of Public Health, The University of Texas Health Science
15 Center at Houston, Houston, TX 77030, USA

16

17 † Contribute equally to this work.

18 * To whom correspondence should be addressed:

19 Zhongming Zhao, Ph.D.

20 Center for Precision Health

21 School of Biomedical Informatics

22 The University of Texas Health Science Center at Houston

23 7000 Fannin St. Suite 600 Houston, TX 77030

24 Phone: 713-500-3631

25 Email: Zhongming.Zhao@uth.tmc.edu

26 **Abstract**

27 **Background:** The coronavirus disease 2019 (COVID-19) is an infectious disease that mainly
28 affects the host respiratory system with ~80% asymptomatic or mild cases and ~5% severe cases.
29 Recent genome-wide association studies (GWAS) have identified several genetic loci associated
30 with the severe COVID-19 symptoms. Delineating the genetic variants and genes is important
31 for better understanding its biological mechanisms.

32 **Methods:** We implemented integrative approaches, including transcriptome-wide association
33 studies (TWAS), colocalization analysis and functional element prediction analysis, to interpret
34 the genetic risks using two independent GWAS datasets in lung and immune cells. To
35 understand the context-specific molecular alteration, we further performed deep learning-based
36 single cell transcriptomic analyses on a bronchoalveolar lavage fluid (BALF) dataset from
37 moderate and severe COVID-19 patients.

38 **Results:** We discovered and replicated the genetically regulated expression of *CXCR6* and *CCR9*
39 genes. These two genes have a protective effect on the lung and a risk effect on whole blood,
40 respectively. The colocalization analysis of GWAS and *cis*-expression quantitative trait loci
41 highlighted the regulatory effect on *CXCR6* expression in lung and immune cells. In the lung
42 resident memory CD8⁺ T (T_{RM}) cells, we found a 3.32-fold decrease of cell proportion and lower
43 expression of *CXCR6* in the severe than moderate patients using the BALF transcriptomic
44 dataset. Pro-inflammatory transcriptional programs were highlighted in T_{RM} cells trajectory from
45 moderate to severe patients.

46 **Conclusions:** *CXCR6* from the *3p21.31* locus is associated with severe COVID-19. *CXCR6*
47 tends to have a lower expression in lung T_{RM} cells of severe patients, which aligns with the
48 protective effect of *CXCR6* from TWAS analysis. We illustrate one potential mechanism of host

49 genetic factor impacting the severity of COVID-19 through regulating the expression of *CXCR6*
50 and T_{RM} cell proportion and stability. Our results shed light on potential therapeutic targets for
51 severe COVID-19.

52 **Keywords: Host genetics, COVID-19, TWAS, colocalization, single cell RNA sequencing,**
53 ***CXCR6*, lung resident memory CD8⁺ T (T_{RM}) cell**

54

55 **Background**

56 The coronavirus disease 2019 (COVID-19) pandemic has already infected over 100
57 million people and caused numerous morbidities and over 2 million death worldwide as of
58 January 2021. The virus is evolving fast with new variants being emerged in the world [1, 2]. A
59 huge disparity in the severity of symptoms in different patients has been observed. In some of the
60 patients, only mild symptoms or even no symptoms are shown and little treatment or
61 interventions are required while a subset of patients experience rapid disease progression to
62 respiratory failure and need urgent and intensive care [3]. Although age and sex are major risk
63 factors of COVID-19 disease severity [4], it remains largely unclear about the factors leading to
64 the variability on COVID-19 severity and which group of individuals confer intrinsic
65 susceptibility to COVID-19.

66 Several genome-wide association studies (GWAS) have been carried out and one
67 genomic risk locus, *3p21.31*, has been replicated to be associated with the critical illness. One
68 recent study by the Severe COVID-19 GWAS Group identified *3p21.31* risk locus for the
69 susceptibility to severe COVID-19 with respiratory failure [5]. This GWAS signal was then
70 replicated in a separate meta-analysis comprising in total 2,972 cases from 9 cohorts by COVID-
71 19 Host Genetics Initiative (HGI) round 4 alpha. However, there is a cluster of 6 genes

72 (*SLC6A20*, *LZTFL1*, *CCR9*, *FYCO1*, *CXCR6*, and *XCRI*) nearby the lead SNP rs35081325
73 within a complex linkage disequilibrium (LD) structure, which makes the “causal” gene and
74 functional implication of this locus remain elusive [5, 6].

75 The majority of GWAS variants are located in non-coding loci, many of which are in the
76 enhancer or promoter regions, playing roles as *cis*- or *trans*- regulatory elements to alter gene
77 expression [7]. Although the function of non-coding variants could not be directly interrupted by
78 their locations, their mediation effect on gene expression could be inferred by the expression
79 quantitative trait loci (eQTL) analysis. In recent years, large consortia like GTEx (Genotype-
80 Tissue Expression), eQTLGen Consortium, and DICE (database of immune cell expression)
81 have generated rich eQTLs resources in diverse tissues and immune-related cell types [7-9]. A
82 variety of statistical approaches such as transcriptome-wide association study (TWAS) analysis
83 and colocalization analysis have successfully interpreted the target genes of non-coding variants
84 by integrating the context-specific eQTLs [10-13].

85 Recent advances in single cell transcriptome sequencing provide unprecedented
86 opportunities to understand the biological mechanism underlying disease pathogenesis at the
87 single cell and cell type levels [14-16]. The recent generation of single cell RNA-sequencing
88 (scRNA-seq) data from the bronchoalveolar lavage fluid (BALF) of moderate and severe
89 COVID-19 patients has revealed the landscape of the gene expression changes in major immune
90 cells. However, the transcriptome alteration in specific subpopulations remains mostly
91 unexplored [17].

92 In this study, we aimed to connect the genetic factors with the context-specific molecular
93 phenotype in COVID-19 patients. As illustrated in **Fig. 1**, we designed a multi-level workflow to
94 dissect the genetically regulated expression (GReX) that contributed to severe COVID-19. We

95 performed TWAS and colocalization analyses with a broad collection of eQTL datasets at the
96 tissue and cellular levels. We further integrated the BALF single cell transcriptome dataset to
97 explore the cellular transcriptome alterations in severe and moderate COVID-19 patients. Lastly,
98 we proposed a hypothetical mechanism, connecting our multi-layer evidence in host genetic
99 factors, gene (*CXCR6*), and single cell transcriptome features with the severity of COVID-19.

100

101 **Methods**

102 **GWAS dataset**

103 We obtained GWAS summary statistics for the phenotype “severe COVID-19 patients vs
104 population” (severe COVID-19) from two separate meta-analyses carried out by the COVID-19
105 Host Genetics Initiative (HGI, <https://www.covid19hg.org/>) and the Severe COVID-19 GWAS
106 Group (SCGG) [5]. The GWAS_{HGI} A2 round 4 (alpha) cohort consists of 12,816,037 SNPs from
107 the association study of 2,972 very severe respiratory confirmed COVID-19 cases and 284,472
108 controls with unknown SARS-CoV-2 infection status from nine independent studies in a
109 majority of the European Ancestry population. The GWAS_{SCGG} dataset is from the first GWAS
110 of severe COVID-19 [5], including 8,431,427 SNPs from the association study conducted from
111 1,980 COVID-19 confirmed patients with severe disease status and 2,205 control participants
112 from two separate cohorts in Europe.

113

114 **Transcriptome-wide association analysis**

115 We performed TWAS analyses of severe COVID-19 using S-PrediXcan [18] to prioritize
116 GWAS findings and identify eQTL-linked genes. S-PrediXcan is a systematic approach that
117 integrates GWAS summary statistics with publicly available eQTL data to translate the evidence

118 of association with a phenotype from the SNP level to the gene level. Briefly, prediction models
119 were built by a flexible and generic approach multivariate adaptive shrinkage in R package
120 (MASHR) using variants with a high probability of being causal for QTL and tissue expression
121 profiles from the GTEx version 8 [7, 19]. We chose three tissues that were relevant to SARS-
122 CoV-2 infection, including lung, whole blood, and spleen. Then, we ran S-PrediXcan scripts
123 (downloaded from <https://github.com/hakyimlab/MetaXcan>, accessed on 10/10/2020) with each
124 of the three tissue-specific models in two severe COVID-19 GWAS datasets respectively. The
125 threshold used in TWAS significance was adjusted by Bonferroni multiple test correction with
126 the ~10,000 genes. We defined the strict significance as $p < 5 \times 10^{-6}$ ($|z| > 4.56$) and suggestive
127 significance as $p < 5 \times 10^{-5}$ ($|z| > 4.06$).

128

129 **Colocalization analysis**

130 Colocalization was performed to validate significant TWAS associations using two recent
131 and cutting-edge statistical analysis approaches: eCAVIAR [20] and fastENLOC [21], which aim
132 to identify a single genetic variant that has shared causality between expression and GWAS trait.
133 Both eCAVIAR and fastENLOC could assess the colocalization posterior probability (CLPP) for
134 two traits at a locus, while eCAVIAR allows for multiple causal variants and fastENLOC
135 features accountability for allelic heterogeneity in expression traits and high sensitivity of the
136 methodology. We ran eCAVIAR between significant TWAS genes and GWAS trait with a
137 maximum of five causal variants per locus and defined a locus as 50 SNPs up- and down- stream
138 of the tested causal variant, following the recommendation in the original paper. The eCAVIAR
139 was downloaded from <https://github.com/fhormoz/caviar/> (accessed on 10/25/2020). The

140 biallelic variants from the 1,000 Genomes Project phase III in European ancestry were used as an
141 LD reference [22]. We defined $CLPP > 0.5$ as having strong colocalization evidence.

142 To run fastENLOC, we first prepared probabilistic eQTL annotations to generate the cis-
143 eQTL's posterior inclusion probability (PIP). Specifically, we applied the tissue-specific data
144 from GTEx and T follicular cell-specific data from the DICE database [9] using the integrative
145 genetic association analysis with the deterministic approximation of posteriors (DAP-G) package
146 [23]. Then, GWAS summary statistics were split into approximately LD-independent regions
147 defined by reference panel from European ancestry and z-scores were converted to PIP. We
148 downloaded the fastENLOC from <https://github.com/xqwen/fastenloc> (accessed on 10/25/2020)
149 and followed the guideline to yield regional colocalization probability (RCP) for each
150 independent GWAS locus using each tissue- or cell type-specific eQTL annotation. We defined
151 $RCP > 0.5$ as having strong colocalization evidence.

152

153 **Functional genomics annotations**

154 To better understand the potential function of the variants identified by GWAS analyses
155 and how they mediate the regulatory effect, we annotated significant SNPs using publicly
156 available data. We obtained the tissue and cellular level eQTL data from the following resources:
157 1) the eQTLGen consortium [24] eQTLs generated from 30,912 whole blood samples; 2)
158 Biobank-based Integrative Omics Studies (BIOS) eQTLs generated from 2,116 healthy adults
159 [25]; 3) The GTEx v8 [7] eQTLs of the lung, whole blood, and spleen tissues; 4) DICE database
160 [9] with cellular eQTLs of 9 available T cell subpopulations. To identify the genomic annotation
161 of the significant SNPs, we downloaded the multivariate hidden Markov model (ChromHMM)
162 [26] processed chromatin-state data of 17 lung and T cell lines from the Roadmap Epigenomics

163 project [27]. To explore the potential chromatin looping of GWAS locus, we used publicly
164 available chromatin interaction (Hi-C) data [28] at a resolution of 40Kb on IMR90, a normal
165 lung fibroblast cell line. The Hi-C data has been used to identify specific baits and targets from
166 distant chromatin regions that frequently interact with each other. Variants within the regulatory
167 regions can be connected to the potential gene targets and thus mediate the gene expression.
168 Statistical tests of bait-target pairs were conducted to define significant bait interaction regions
169 and their targets. The eQTL associations and chromatin-state information and Hi-C interactions
170 were processed and plotted using the R Bioconductor package *gviz* in R version 4.0.3 [29].

171

172 **Differentially expressed gene analysis in resident memory CD8⁺ T cells**

173 We use the recently published scRNA-seq dataset of bronchoalveolar lavage fluids
174 (BALF) samples from nine patients (three moderate and six severe) with COVID-19 [17, 30].
175 We adapted the original annotation [17] and followed their method to calculate the resident
176 memory CD8⁺ T (T_{RM}) cells signature score by using 31 markers (14 positive markers and 17
177 negative markers) for all annotated CD8⁺ T cells [31, 32]. We excluded cells with CD4⁺
178 expression and defined the top 50% scored cells as the T_{RM} cells. Lastly, we conducted a non-
179 parametric Wilcoxon rank sum test by the function of “FindAllMarkers” from R package Seurat
180 [33](version 3.1.5 in R version 3.5.2) to perform the differentially expressed genes (DEG)
181 analysis between moderate and severe patients.

182

183 **Cell trajectory and transcriptional program analysis in T_{RM} cells**

184 We used the R package Slingshot [34] to infer cell transition and pseudotime from the scRNA-
185 seq data. Specifically, we first used the expression data to generate the minimum spanning tree

186 of cells in a reduced-dimensionality space [t-Distributed Stochastic Neighbor Embedding (tSNE)
187 project from top 30 principle components of top 3,000 variable genes] assuming there are two
188 major clusters (moderate and severe T_{RM} cells). We then applied the principal curve algorithm
189 [35] to infer an one-dimensional variable (pseudotime) representing the each cell's trajectory
190 along the transcriptional progression. We used our in-house machine learning tool, DrivAER
191 (Driving transcriptional programs based on AutoEncoder derived relevance scores) [36], to
192 identify potential transcriptional programs (e.g., gene sets of pathways or transcription factors
193 (TF)s) that potentially regulate the inferred cell trajectory between the moderate and severe
194 patients. To avoid the potential noise from the low expression genes, we excluded those genes
195 expressed in < 10% cells. DrivAER took gene-expression and pseudotime inferred from previous
196 cell trajectory results (Slingshot) and calculated each gene's relevance score by performing
197 cellular manifold by using Deep Count Autoencoder [37] and a random forest model with out-of-
198 bag score calculation as the relevance score. The transcriptional program annotations were from
199 the hallmark pathway gene sets from MSigDB [38] and transcription factor (TF) target gene sets
200 from TRRUST [39]. To calculate the relevance score, we used the “calc_relevance” function
201 with the following parameters: min_targets = 10, ae_type = “nb-conddisp”, epoch=100,
202 early_stop=3, and hidden_size = “(8,2,8)”. The relevance score (R² coefficient of determination)
203 indicates the proportion of variance in the pseudotime explained by target genes of transcription
204 factor or genes in the hallmark pathways.

205

206 **DNA motif recognition analysis of genome-wide significant SNPs**

207 We used the function “variation-scan” of the online tool RSAT ([http://rsat.sb-](http://rsat.sb-roscoff.fr/index.php)
208 [roscoff.fr/index.php](http://rsat.sb-roscoff.fr/index.php), accessed on 01/15/2020) [40] to predict the binding effect of all the

209 significant SNPs at the *3p21.31* locus. We defined the TF with Bonferroni corrected $p < 0.05$ as
210 the significant TF. Later, we compared them with the TF with high relevance score from the
211 DrivAER analysis above. The position weight matrices (PWMs) for all the TFs were
212 downloaded from cis-BP Database (<http://cisbp.ccb.utoronto.ca/>) version 2019-06_v2.00 [41]
213 and sequence logos representing motif binding sites were generated using R package seqLogo
214 version 1.54.3 in R version 3.5.2.

215

216 **Results**

217 **TWAS analysis identified and replicated two chemokine receptor genes**

218 We utilized the latest S-PrediXcan MASHR models trained with GTEx v8 data for
219 TWAS analyses in lung and whole blood on two GWAS datasets of susceptibility to severe
220 COVID-19 [19]. In the HGI cohort, we found that a decreased expression of *CXCR6*, which
221 encodes C-X-C chemokine receptor type 6, in the lung was associated with an increased risk for
222 the development of severe COVID-19 symptoms ($p = 1.57 \times 10^{-17}$, $z = -8.53$), and this result was
223 then replicated in the SCGG cohort ($p = 2.84 \times 10^{-5}$, $z = -4.19$, suggestive significant) (**Fig. 2** and
224 **Table 1**). Likewise, an increased expression of *CCR9*, which encodes C-C chemokine receptor
225 type 9, in whole blood was associated with an increased risk for the development of severe
226 COVID-19 complications in GWAS_{HGI} cohort ($p = 7.90 \times 10^{-11}$, $z = 6.50$) and this result was
227 replicated in the other GWAS_{SCGG} cohort, ($p = 3.78 \times 10^{-10}$, $z = 6.26$) (**Fig. 2** and **Table 1**).

228 Whole blood and lung transcriptome models also identified two additional significant TWAS
229 genes that are specific to one of the two cohorts. Increased expression of *ABO* gene in the lung
230 was associated with risk for the development of severe COVID-19 symptoms in GWAS_{SCGG} data
231 set ($p = 5.98 \times 10^{-7}$, $z = 4.99$). Similarly, increased expression of *GAS7* gene (Growth Arrest-

232 Specific 7) in whole blood was associated with an increased risk for development of COVID-19
233 symptom in the GWAS_{HGI} data set ($p = 8.46 \times 10^{-7}$, $z = 4.92$). Overall, these two chemokine
234 receptor genes were found and replicated to be associated with COVID-19 and we used them for
235 further downstream analyses.

236

237 **Colocalization analysis validated the mediation effect of *CXCR6* between GWAS locus and** 238 **severe COVID-19**

239 The TWAS findings might be driven by pleiotropy or linkage effect by the LD structure
240 in the GWAS loci instead of the true mediation effect [42] (**Fig. 3a**). To rule out the linkage
241 effect and find further evidence of true colocalization of causal signals in the variants that were
242 significant in both GWAS and eQTL analyses, we performed colocalization analysis by
243 eCAVIAR and fastENLOC using several tissue-specific eQTL datasets. The eCAVIAR with the
244 eQTL data in lung tissue revealed that the severe COVID-19 association could be mediated by
245 the variants that were associated with the expression of *CXCR6* (CLPP = 0.79) (**Table 1**). And
246 the colocalized SNP rs34068335 (GWAS_{HGI} $p = 5.02 \times 10^{-22}$) is also related to the increased
247 monocyte percentage of white cells in a blood-trait GWAS study using Phenoscanner [43-45].
248 The fastENLOC analysis showed a high RCP between the expression of *CXCR6* in T follicular
249 helper cells and GWAS signal in both the GWAS_{HGI} cohort (RCP=0.99) and the GWAS_{SCGG}
250 cohort (RCP = 0.99) (**Table 1**). However, colocalization analysis of *CCR9* did not suggest strong
251 colocalization evidence (CLPP < 0.1 and RCP < 0.1).

252

253 **Multi-level functional annotations linked *3p21.31* locus with *CXCR6* and *CCR9* functions**

254 To explore the potential functions linked with the GWAS risk variants, we examined the
255 functional genomic annotations in this locus. Specifically, we found a consistent decreasing
256 effect of *CXCR6* expression in T cells and whole blood from the two large-scaled eQTL datasets
257 (**Fig. 3b**). Furthermore, multiple SNPs at the *3p21.31* locus reside in the annotated regulatory
258 elements across blood, T cell, and lung cell lines (**Fig. 3c**, Methods). The Hi-C cell line data
259 from lung fibroblast [28] also showed a significant interaction between the *3p21.31* locus had
260 interactions with both *CXCR6* and *CCR9* promoter regions (**Fig. 3d**). Overall, these results from
261 the multiple lines of evidence all supported the potential regulatory effects of the *3p21.31* locus
262 on *CXCR6* expression.

263

264 ***CXCR6* differentially expressed in T_{RM} cells of severe and moderate patients**

265 According to our tissue cell-type-specific expression database (CSEA-DB), *CXCR6* is
266 mainly expressed in immune cells in human lung tissue (e.g., T cell and NK cell) [16]. In Liao et
267 al.'s work, the authors reported that *CXCR6* had lower expression in severe patients than
268 moderate patients, indicating a potential protective effect in T cells of human respiratory systems
269 [17]. However, T cells have various resident and circulating subtypes with diverse functions
270 [46]. To understand which subpopulation(s) of T cells might be associated with the severity of
271 COVID-19, we used the BLAF scRNA-seq data of six severe patients and three moderate
272 patients. The data included 6,491 T-cells (4,356 from six severe patients and 2,135 from three
273 moderate patients). We further used a set of 31 T_{RM} cell marker genes to distinguish the T_{RM}
274 cells and conventional CD8⁺ T cells (Methods). As shown in **Fig. 4a and 4b**, the T_{RM} cells and
275 conventional T cells could be distinguished in both moderate and severe patients with the classic
276 T_{RM} cells markers (*CXCR6* [31], CD69 [47], *ITGAE* (the gene encoding CD103) [47, 48],

277 *ZNF683* [48], and *XCL1* [46]) and three negative-control markers (*SELL* (the gene encoding
278 CD62L) [47], *KLF2*, and *S1PR1* [49]) from previous study [31]. Among the 1,090 lung T_{RM}
279 cells, we found that 675 cells were from moderate patients and only 415 cells were from severe
280 patients. This represented a 3.32-fold decrease for the expected number of T_{RM} cells in severe
281 patients. We used the non-parametric Wilcoxon rank sum test to identify the DEGs in the T_{RM}
282 cells between severe and moderate patients and found *CXCR6* had significantly lower expression
283 in the severe patients than the moderate patients ($p < 2.5 \times 10^{-16}$, fold change = 1.57, **Fig. 4c**).

284

285 **Inferring the transcriptional programs that drive the cell status transition**

286 To understand the transition between moderate and severe T_{RM} cells, we constructed the
287 cell trajectory/pseudotime along with T_{RM} cells by using Slingshot (**Fig. 4d**) [34]. Next, we
288 applied our DrivAER approach (Driving transcriptional programs based on AutoEncoder derived
289 Relevance scores) [36] to identify the potential transcriptional programs that were most likely
290 involved in the cell trajectory/pseudotime. **Fig. 4e** shows a scaled heatmap to demonstrate the
291 relative expression of naïve and effector markers of T cells in the order of pseudotime generated
292 by Slingshot [34, 39]. We identified that the severe T_{RM} cells were mainly gathered in the later
293 stage of the pseudotime. The naïve markers (*IL7R*, *BCL2*) were higher expressed in moderate
294 patients than in severe patients (except *SELL*). On the contrary, some effector markers (*GZMB*,
295 *HAVCR2*, *LAG3*, *IFNG*) were lower expressed in moderate patients than in severe patients. Other
296 effector markers (*IRF4*, *PRFI*) had higher expression in the middle of the transition than their
297 expression at the start and end sides. These results indicated that the T_{RM} cells in severe patients
298 still in pro-inflammatory status although the T_{RM} cells status were more heterogeneous in severe
299 patients than in moderate patients (**Fig. 4a, 4b, and 4e**). As shown in **Fig. 4f and 4g**, the top five

300 molecular signatures (relevance score > 0.25) identified by DrivAER included T-cell pro-
301 inflammatory actions (interferon gamma response, allograft rejection [50], interferon alpha
302 response, and complement system) as well as proliferative mTORC1 signaling pathway [51].
303 Among the top TFs (relevance score > 0.25) that drove this cell trajectory, the DNA binding
304 RELA-NFKB1 complex is involved in several biological processes, such as inflammation,
305 immunity, and cell growth initiated by external stimuli. The signal transducer and activator of
306 transcription (*STAT1*) and its regulator histone deacetylase (*HDAC1*) could be activated by
307 various ligands including interferon-alpha and interferon-gamma. In summary, the TF results are
308 well consistent with our previous hallmark pathway findings (**Additional file: Table S1 and**
309 **Table S2**).

310

311 **Several genome-wide significant SNPs might change the TF binding site affinity**

312 To understand the potential TF binding affinity changes of genome-wide significant
313 SNPs, we conducted the DNA motif recognition analysis of the seven TFs related to the
314 transcriptional program between moderate and severe T_{RM} cells (relevance score > 0.25,
315 **Additional file 1: Table S2**). We identified SNP rs10490770 [T/C, minor allele frequency
316 (MAF) = 0.097, GWAS_{HGI} = 9.53×10^{-39}] and SNP rs67959919 (G/A, MAF = 0.097, GWAS_{HGI}
317 = 8.83×10^{-39}) that were predicted to alter the binding affinity of TFs RELA and SP1,
318 respectively (**Additional file 1: Fig. S1a and S1b**). Moreover, these two SNPs were in the high
319 LD region ($r^2 > 0.8$) with several significant lead eQTLs (SNP rs35896106 and rs17713054) of
320 *CXCR6* in whole blood ($p = 5.03 \times 10^{-37}$) and T follicular helper cell ($p = 1.30 \times 10^{-5}$) (**Fig. 3b**).
321 In summary, the genome-wide significant SNPs were predicted to change the binding affinity of

322 those TFs highly related to T_{RM} cells status transition, (**Additional file 2: Table S3**), suggesting
323 their potential regulation of *CXCR6* expression.

324

325 **Discussion**

326 In this work, we developed a multi-level, integrative genetic and functional analysis
327 framework to explore the host genetic factors on the expression change of GWAS-implicated
328 genes for COVID-19 severity. Specifically, we conducted TWAS analysis for two independent
329 COVID-19 GWAS datasets. We identified and replicated two chemokine receptor genes, *CXCR6*
330 and *CCR9*, with a protective effect in the lung and a risk effect in whole blood, respectively.
331 *CXCR6* is expressed in T lymphocytes and essential genes in $CD8^+$ T_{RM} cells, mediating the
332 homing of T_{RM} cells to the lung along with its ligand *CXCL16* [52, 53]. *CCR9* was reported to
333 regulate chemotaxis in response to thymus-expressed chemokine in T cells [54]. The
334 colocalization analysis identified that both GWAS and eQTLs of *CXCR6* had high colocalization
335 probabilities in the lung, whole blood, and T follicular helper cells, which confirms the genetic
336 regulation roles at this locus. At the single cell level, our DEG analysis identified *CXCR6* gene
337 had lower expression in the COVID-19 severe patients than the moderate patients in both T cells
338 and T_{RM} cells, supporting its protective effect identified in TWAS analysis in lung and whole
339 blood. The expected proportion of T_{RM} cells also decreased by 3.32-fold (**Table 2**). Interestingly,
340 these findings were replicated in circulating $CXCR6^+$ $CD8^+$ T cells of severe and control/mild
341 patients by flow cytometry experiment [53]. We identified the major transition force from
342 moderate T_{RM} cells to severe T_{RM} cells are pro-inflammatory pathways and TFs.

343 From the TWAS and colocalization analysis in lung and immune cells, we successfully
344 replicated that *CXCR6* was centered in the GWAS signal at locus *3p21.31*. Previous studies have

345 reported that *CXCR6*^{-/-} significantly decreases airway lung T_{RM} cells due to altered trafficking of
346 *CXCR6*^{-/-} cells within the lung of the mice [52], which could explain a much less proportion of
347 T_{RM} cells in severe patients than moderate patients. The lung T_{RM} cells provide the first line of
348 defense against infection and coordinate the subsequent adaptive response [55]. The previous
349 study has reported that T_{RM} cells constitutively expressed surface receptors (PD-1 and CTLA-4)
350 that are associated with inhibition of T cell function, which might prevent excessive activation or
351 inflammation in the tissue niche [56].

352 We further used nine classic naïve markers (e.g., *BCL2*, *SELL*, *TCF7*, and *IL7R*) and ten
353 classic effector markers (e.g., *GZMB*, *PRF1*, *IFNG*, *LAG3*, and *PDCD1*) to quantify the naïve
354 and effector status of the T_{RM} cells (**Additional file 1: Fig. S2**). T_{RM} cells in severe patients had
355 a much higher median of effector marker score (0.44 in severe and 0.18 in moderate T_{RM} cells)
356 than T_{RM} cells in moderate patients did, suggesting that the severe T_{RM} cells had much higher
357 activities in inflammation as we discovered in **Fig. 4f** despite their proportion decrease. For the
358 naïve score (**Additional file 1: Fig. S2**), both moderate and severe T_{RM} cells had limited
359 expressions (median score: 0.028 in severe and 0.038 in moderate T_{RM} cells). Interestingly, if we
360 removed the lymph node homing receptor *SELL* [31] from the naïve markers list, we would find
361 the median score in severe naïve markers would drop to 0 (**Additional file 1: Fig. S2**). This
362 indicated that *SELL* expression contributed greatly to the naïve status of T_{RM} severe patients.
363 Consistently in **Fig. 4e**, we could also observe that a large proportion of T_{RM} cells had higher
364 *SELL* expression in severe patients than in moderate patients, suggesting the T_{RM} cells in severe
365 patients might not be in a stable cell status due to the lymph node homing signal (*SELL*). To this
366 end, we hypothesized that genetically lower expressed *CXCR6* would decrease the proportion of
367 T_{RM} cells residing in the lung through the *CXCR6*/*CXCL16* axis [52, 53], impairing the first-line

368 defense. Moreover, the lower expression of *CXCR6* would also lead to the “unstable” residency
369 of T_{RM} cells in lung (**Fig. 4b**). The T_{RM} cells play essential roles for orchestrating the immune
370 system, lack of which would lead to severe COVID-19 symptoms, such as acute respiratory
371 distress syndrome, cytokine storm and major multi-organ damage [57] (**Fig. 5**).

372 In this study, we mainly focused on the multi-evidence validated gene *CXCR6* and its
373 mechanism related to severe COVID-19. Although we are unable to directly test the genotype of
374 those severe patients, the association of the single cell level phenotype (lower expression of
375 *CXCR6* and decreased proportion of CD8⁺ *CXCR6*⁺ T cells) and the severe COVID-19 has been
376 observed in another work with flow cytometry experiments [53]. We are aware of the genetic
377 factors on *CXCR6* might only explain a proportion of the severe COVID-19 variance. Other
378 genetic mechanisms discovered in GWAS and TWAS analyses need further exploration [6]. The
379 GWAS_{HGI} dataset used in this study was HGI round 4 (alpha), which was the largest GWAS by
380 the access date of October 20, 2020. However, it was not the currently largest GWAS meta-
381 analysis for severe COVID-19 when we prepared the manuscript. This research field is evolving
382 very fast, due to the urgent demand of public health. Currently, the largest GWAS HGI round 4
383 (freeze) contained more samples (4,336 cases/ 353,891 controls), and it included two
384 independent datasets we used in this study. Considering that the GWAS_{HGI} dataset included
385 ~10% control samples from the Asian population, we checked the LocusZoom plot of the chr3:
386 45.80-46.40 million base pairs (Mb) region on GRCh37 reference genome. We found a
387 consistent tendency in GWAS round 4 alpha and freeze version (**Additional file1: Fig. S3**).
388 Another limitation is that the scRNA-seq data only had nine COVID-19 patient samples (six
389 severe and three moderate samples), which might not provide enough statistical power at the
390 sample level as it is commonly considered each scRNA-seq data acts like a population. Finally,

391 the TF binding site affinity alterations were assessed based on computational prediction,
392 therefore, the *in vivo* effects require experimental validation. We anticipate more and larger
393 datasets will be released in the near future. We will apply our integrative analysis approach to
394 such new data.

395

396 **Conclusions**

397 Our work systematically explored the genetic effect on gene expression at chromosome
398 locus *3p21.31* and pinpointed the gene *CXCR6* might be involved in the severity of COVID-19.
399 Several genome-wide significant SNPs were within the LD block of *CXCR6* eQTLs in immune-
400 related cells. In a scRNA-seq COVID-19 BALF dataset, we characterized that *CXCR6* (T_{RM} cells
401 marker gene) had a lower expression in severe patients than in moderate patients. Moreover, the
402 T_{RM} cells in severe patients had a 3.32-fold proportion decrease and much higher pro-
403 inflammatory activity than T_{RM} cells in moderate patients. Based on these observations, we
404 proposed a potential mechanism on how the lower expression of *CXCR6* regulated by the
405 endogenous factors could progress to severe COVID-19 outcomes.

406

407 **List of abbreviations**

408 BALF: bronchoalveolar lavage fluid; BIOS: Biobank-based Integrative Omics Studies;
409 ChromHMM: chromatin-state hidden Markov model; COVID-19: coronavirus disease 2019;
410 CLPP: colocalization posterior probability; CSEA-DB: cell-type-specific expression database;
411 DAP: deterministic approximation of posteriors; DEG: differentially expressed gene; DICE:
412 database of immune cell expression; DrivAER: Driving transcriptional programs based on
413 AutoEncoder derived Relevance scores; eQTL: expression quantitative trait; GReX: genetically

414 regulated expression; GWAS: genome-wide association study; HGI: Host Genetics Initiative; Hi-
415 C: high-throughput chromatin interaction; LD: linkage disequilibrium; MAF: minor allele
416 frequency; MASHR: multivariate adaptive shrinkage in R; Mb: million base pairs; MSigDB:
417 molecular signatures database; PIP: posterior inclusion probability; PWM: position weight
418 matrix; SARS-CoV-2: severe acute respiratory syndrome coronavirus 2; RCP: regional
419 colocalization probability; SCGG: Severe COVID-19 GWAS Group; scRNA-seq: single cell
420 RNA sequencing; tSNE: t-Distributed Stochastic Neighbor Embedding; TF: transcription factor;
421 T_{RM} cells: resident memory CD8⁺ T cells; TWAS: transcriptome-wide association study;

422

423 **Funding**

424 Dr. Zhao was partially supported by National Institutes of Health grant R01LM012806 and Chair
425 Professorship for Precision Health funds. We thank the technical support from the Cancer
426 Genomics Core funded by the Cancer Prevention and Research Institute of Texas (CPRIT
427 RP180734). The funders had no role in the study design, data collection and analysis, decision to
428 publish, or preparation of the manuscript.

429 **Acknowledgements**

430 We appreciate Drs. Teng Liu and Dawei Zou for the valuable comments. We thank all members
431 of the Bioinformatics and Systems Medicine Laboratory for the discussion.

432

433

434 References

- 435 1. Zhao Z, Li H, Wu X, Zhong Y, Zhang K, Zhang YP, Boerwinkle E, Fu YX: **Moderate**
436 **mutation rate in the SARS coronavirus genome and its implications.** *BMC Evol Biol*
437 2004, **4**:21.
- 438 2. Liu S, Shen J, Fang S, Li K, Liu J, Yang L, Hu CD, Wan J: **Genetic Spectrum and Distinct**
439 **Evolution Patterns of SARS-CoV-2.** *Front Microbiol* 2020, **11**:593548.
- 440 3. Wu Z, McGoogan JM: **Characteristics of and Important Lessons From the Coronavirus**
441 **Disease 2019 (COVID-19) Outbreak in China: Summary of a Report of 72314 Cases**
442 **From the Chinese Center for Disease Control and Prevention.** *JAMA* 2020, **323**:1239-
443 1242.
- 444 4. Bhopal SS, Bhopal R: **Sex differential in COVID-19 mortality varies markedly by age.** vol.
445 396. pp. 532-533: Lancet Publishing Group; 2020:532-533.
- 446 5. Severe Covid GG, Ellinghaus D, Degenhardt F, Bujanda L, Buti M, Albillos A, Invernizzi P,
447 Fernandez J, Prati D, Baselli G, et al: **Genomewide Association Study of Severe Covid-19**
448 **with Respiratory Failure.** *N Engl J Med* 2020, **383**:1522-1534.
- 449 6. Pairo-Castineira E, Clohisey S, Klaric L, Bretherick AD, Rawlik K, Pasko D, Walker S,
450 Parkinson N, Fourman MH, Russell CD, et al: **Genetic mechanisms of critical illness in**
451 **Covid-19.** *Nature* 2020.
- 452 7. GTEx Consortium: **The GTEx Consortium atlas of genetic regulatory effects across**
453 **human tissues.** *Science* 2020, **369**:1318-1330.
- 454 8. Võsa U, Claringbould A, Westra H-J, Bonder MJ, Deelen P, Zeng B, Kirsten H, Saha A,
455 Kreuzhuber R, Kasela S, et al: **Unraveling the polygenic architecture of complex traits**
456 **using blood eQTL metaanalysis.** *bioRxiv* 2018:447367.
- 457 9. Schmiedel BJ, Singh D, Madrigal A, Valdovino-Gonzalez AG, White BM, Zapardiel-
458 Gonzalo J, Ha B, Altay G, Greenbaum JA, McVicker G, et al: **Impact of Genetic**
459 **Polymorphisms on Human Immune Cell Gene Expression.** *Cell* 2018, **175**:1701-1715
460 e1716.
- 461 10. Gamazon ER, Wheeler HE, Shah KP, Mozaffari SV, Aquino-Michaels K, Carroll RJ, Eyler
462 AE, Denny JC, Consortium GT, Nicolae DL, et al: **A gene-based association method for**
463 **mapping traits using reference transcriptome data.** *Nat Genet* 2015, **47**:1091-1098.
- 464 11. Giambartolomei C, Vukcevic D, Schadt EE, Franke L, Hingorani AD, Wallace C, Plagnol V:
465 **Bayesian test for colocalisation between pairs of genetic association studies using**
466 **summary statistics.** *PLoS Genet* 2014, **10**:e1004383.
- 467 12. Dai Y, Pei G, Zhao Z, Jia P: **A Convergent Study of Genetic Variants Associated With**
468 **Crohn's Disease: Evidence From GWAS, Gene Expression, Methylation, eQTL and**
469 **TWAS.** *Front Genet* 2019, **10**:318.
- 470 13. Dai Y, Hu R, Pei G, Zhang H, Zhao Z, Jia P: **Diverse types of genomic evidence converge**
471 **on alcohol use disorder risk genes.** *J Med Genet* 2020, **57**:733-743.
- 472 14. Mathys H, Davila-Velderrain J, Peng Z, Gao F, Mohammadi S, Young JZ, Menon M, He L,
473 Abdurrob F, Jiang X, et al: **Single-cell transcriptomic analysis of Alzheimer's disease.**
474 *Nature* 2019, **570**:332-337.
- 475 15. Papalexi E, Satija R: **Single-cell RNA sequencing to explore immune cell heterogeneity.**
476 *Nat Rev Immunol* 2018, **18**:35-45.

- 477 16. Dai Y, Hu R, Manuel AM, Liu A, Jia P, Zhao Z: **CSEA-DB: an omnibus for human complex**
478 **trait and cell type associations.** *Nucleic Acids Res* 2021, **49**:D862-D870.
- 479 17. Liao M, Liu Y, Yuan J, Wen Y, Xu G, Zhao J, Cheng L, Li J, Wang X, Wang F, et al: **Single-**
480 **cell landscape of bronchoalveolar immune cells in patients with COVID-19.** *Nat Med*
481 2020, **26**:842-844.
- 482 18. Barbeira AN, Dickinson SP, Bonazzola R, Zheng J, Wheeler HE, Torres JM, Torstenson ES,
483 Shah KP, Garcia T, Edwards TL, et al: **Exploring the phenotypic consequences of tissue**
484 **specific gene expression variation inferred from GWAS summary statistics.** *Nature*
485 *Communications* 2018, **9**:1-20.
- 486 19. Urbut SM, Wang G, Carbonetto P, Stephens M: **Flexible statistical methods for**
487 **estimating and testing effects in genomic studies with multiple conditions.** *Nat Genet*
488 2019, **51**:187-195.
- 489 20. Hormozdiari F, van de Bunt M, Segrè AV, Li X, Joo JWW, Bilow M, Sul JH, Sankararaman S,
490 Pasaniuc B, Eskin E: **Colocalization of GWAS and eQTL Signals Detects Target Genes.**
491 *American Journal of Human Genetics* 2016, **99**:1245-1260.
- 492 21. Wen X, Pique-Regi R, Luca F: **Integrating molecular QTL data into genome-wide genetic**
493 **association analysis: Probabilistic assessment of enrichment and colocalization.** *PLOS*
494 *Genetics* 2017, **13**:e1006646-e1006646.
- 495 22. Genomes Project C, Auton A, Brooks LD, Durbin RM, Garrison EP, Kang HM, Korbel JO,
496 Marchini JL, McCarthy S, McVean GA, Abecasis GR: **A global reference for human**
497 **genetic variation.** *Nature* 2015, **526**:68-74.
- 498 23. Lee Y, Luca F, Pique-Regi R, Wen X: **Bayesian Multi-SNP genetic association analysis:**
499 **Control of FDR and use of summary statistics.** pp. 316471-316471: bioRxiv;
500 2018:316471-316471.
- 501 24. Võsa U, Claringbould A, Westra HJ, Bonder MJ, Deelen P, Zeng B, Kirsten H, Saha A,
502 Kreuzhuber R, Kasela S, et al: **Unraveling the polygenic architecture of complex traits**
503 **using blood eQTL meta-analysis.** vol. 18. pp. 10-10: bioRxiv; 2018:10-10.
- 504 25. Zhernakova DV, Deelen P, Vermaat M, van Iterson M, van Galen M, Arindrarto W, van 't
505 Hof P, Mei H, van Dijk F, Westra HJ, et al: **Identification of context-dependent**
506 **expression quantitative trait loci in whole blood.** *Nat Genet* 2017, **49**:139-145.
- 507 26. Ernst J, Kellis M: **ChromHMM: automating chromatin-state discovery and**
508 **characterization.** *Nat Methods* 2012, **9**:215-216.
- 509 27. Roadmap Epigenomics C, Kundaje A, Meuleman W, Ernst J, Bilenky M, Yen A, Heravi-
510 Moussavi A, Kheradpour P, Zhang Z, Wang J, et al: **Integrative analysis of 111 reference**
511 **human epigenomes.** *Nature* 2015, **518**:317-329.
- 512 28. Dixon JR, Selvaraj S, Yue F, Kim A, Li Y, Shen Y, Hu M, Liu JS, Ren B: **Topological domains**
513 **in mammalian genomes identified by analysis of chromatin interactions.** *Nature* 2012,
514 **485**:376-380.
- 515 29. Hahne F, Ivanek R: **Visualizing genomic data using Gviz and bioconductor.** In *Volume*
516 1418: Humana Press Inc.; 2016: 335-351
- 517 30. Liu T, Jia P, Fang B, Zhao Z: **Differential Expression of Viral Transcripts From Single-Cell**
518 **RNA Sequencing of Moderate and Severe COVID-19 Patients and Its Implications for**
519 **Case Severity.** *Front Microbiol* 2020, **11**:603509.

- 520 31. Kumar BV, Ma W, Miron M, Granot T, Guyer RS, Carpenter DJ, Senda T, Sun X, Ho SH,
521 Lerner H, et al: **Human Tissue-Resident Memory T Cells Are Defined by Core**
522 **Transcriptional and Functional Signatures in Lymphoid and Mucosal Sites.** *Cell Rep*
523 2017, **20**:2921-2934.
- 524 32. Pont F, Tosolini M, Fournie JJ: **Single-Cell Signature Explorer for comprehensive**
525 **visualization of single cell signatures across scRNA-seq datasets.** *Nucleic Acids Res*
526 2019, **47**:e133.
- 527 33. Stuart T, Butler A, Hoffman P, Hafemeister C, Papalexi E, Mauck WM, 3rd, Hao Y,
528 Stoeckius M, Smibert P, Satija R: **Comprehensive Integration of Single-Cell Data.** *Cell*
529 2019, **177**:1888-1902 e1821.
- 530 34. Street K, Risso D, Fletcher RB, Das D, Ngai J, Yosef N, Purdom E, Dudoit S: **Slingshot: cell**
531 **lineage and pseudotime inference for single-cell transcriptomics.** *BMC Genomics* 2018,
532 **19**:477.
- 533 35. Hastie T, Stuetzle W: **Principal Curves.** *Journal of the American Statistical Association*
534 1989, **84**:502-516.
- 535 36. Simon LM, Yan F, Zhao Z: **DrivAER: Identification of driving transcriptional programs in**
536 **single-cell RNA sequencing data.** *Gigascience* 2020, **9**.
- 537 37. Eraslan G, Simon LM, Mircea M, Mueller NS, Theis FJ: **Single-cell RNA-seq denoising**
538 **using a deep count autoencoder.** *Nat Commun* 2019, **10**:390.
- 539 38. Liberzon A, Birger C, Thorvaldsdottir H, Ghandi M, Mesirov JP, Tamayo P: **The Molecular**
540 **Signatures Database (MSigDB) hallmark gene set collection.** *Cell Syst* 2015, **1**:417-425.
- 541 39. Han H, Cho JW, Lee S, Yun A, Kim H, Bae D, Yang S, Kim CY, Lee M, Kim E, et al: **TRRUST**
542 **v2: an expanded reference database of human and mouse transcriptional regulatory**
543 **interactions.** *Nucleic Acids Res* 2018, **46**:D380-D386.
- 544 40. Nguyen NTT, Contreras-Moreira B, Castro-Mondragon JA, Santana-Garcia W, Ossio R,
545 Robles-Espinoza CD, Bahin M, Collombet S, Vincens P, Thieffry D, et al: **RSAT 2018:**
546 **regulatory sequence analysis tools 20th anniversary.** *Nucleic Acids Res* 2018, **46**:W209-
547 W214.
- 548 41. Weirauch MT, Yang A, Albu M, Cote AG, Montenegro-Montero A, Drewe P, Najafabadi
549 HS, Lambert SA, Mann I, Cook K, et al: **Determination and inference of eukaryotic**
550 **transcription factor sequence specificity.** *Cell* 2014, **158**:1431-1443.
- 551 42. Wainberg M, Sinnott-Armstrong N, Mancuso N, Barbeira AN, Knowles DA, Golan D,
552 Ermel R, Ruusalepp A, Quertermous T, Hao K, et al: **Opportunities and challenges for**
553 **transcriptome-wide association studies.** *Nat Genet* 2019, **51**:592-599.
- 554 43. Astle WJ, Elding H, Jiang T, Allen D, Ruklisa D, Mann AL, Mead D, Bouman H, Riveros-
555 Mckay F, Kostadima MA, et al: **The Allelic Landscape of Human Blood Cell Trait**
556 **Variation and Links to Common Complex Disease.** *Cell* 2016, **167**:1415-1429.e1419.
- 557 44. Kamat MA, Blackshaw JA, Young R, Surendran P, Burgess S, Danesh J, Butterworth AS,
558 Staley JR: **PhenoScanner V2: An expanded tool for searching human genotype-**
559 **phenotype associations.** *Bioinformatics* 2019, **35**:4851-4853.
- 560 45. Staley JR, Blackshaw J, Kamat MA, Ellis S, Surendran P, Sun BB, Paul DS, Freitag D,
561 Burgess S, Danesh J, et al: **PhenoScanner: A database of human genotype-phenotype**
562 **associations.** *Bioinformatics* 2016, **32**:3207-3209.

- 563 46. Hombrink P, Helbig C, Backer RA, Piet B, Oja AE, Stark R, Brassler G, Jongejan A, Jonkers
564 RE, Nota B, et al: **Programs for the persistence, vigilance and control of human CD8(+)**
565 **lung-resident memory T cells.** *Nat Immunol* 2016, **17**:1467-1478.
- 566 47. Martin MD, Badovinac VP: **Defining Memory CD8 T Cell.** *Front Immunol* 2018, **9**:2692.
- 567 48. Wauters E, Van Mol P, Garg AD, Jansen S, Van Herck Y, Vanderbeke L, Bassez A, Boeckx
568 B, Malengier-Devlies B, Timmerman A, et al: **Discriminating mild from critical COVID-19**
569 **by innate and adaptive immune single-cell profiling of bronchoalveolar lavages.** *Cell*
570 *Res* 2021.
- 571 49. Skon CN, Lee JY, Anderson KG, Masopust D, Hogquist KA, Jameson SC: **Transcriptional**
572 **downregulation of S1pr1 is required for the establishment of resident memory CD8+ T**
573 **cells.** *Nat Immunol* 2013, **14**:1285-1293.
- 574 50. Benichou G, Gonzalez B, Marino J, Ayasoufi K, Valujskikh A: **Role of Memory T Cells in**
575 **Allograft Rejection and Tolerance.** *Front Immunol* 2017, **8**:170.
- 576 51. Yu JS, Cui W: **Proliferation, survival and metabolism: the role of PI3K/AKT/mTOR**
577 **signalling in pluripotency and cell fate determination.** *Development* 2016, **143**:3050-
578 3060.
- 579 52. Wein AN, McMaster SR, Takamura S, Dunbar PR, Cartwright EK, Hayward SL, McManus
580 DT, Shimaoka T, Ueha S, Tsukui T, et al: **CXCR6 regulates localization of tissue-resident**
581 **memory CD8 T cells to the airways.** *J Exp Med* 2019, **216**:2748-2762.
- 582 53. Payne DJ, Dalal S, Leach R, Parker R, Griffin S, McKimmie CS, Cook GP, Richards SJ,
583 Hillmen P, Munir T, et al: **The CXCR6/CXCL16 axis links inflamm-aging to disease**
584 **severity in COVID-19 patients.** *bioRxiv* 2021:2021.2001.2025.428125.
- 585 54. Lee HS, Kim HR, Lee EH, Jang MH, Kim SB, Park JW, Seoh JY, Jung YJ: **Characterization of**
586 **CCR9 expression and thymus-expressed chemokine responsiveness of the murine**
587 **thymus, spleen and mesenteric lymph node.** *Immunobiology* 2012, **217**:402-411.
- 588 55. Ardain A, Marakalala MJ, Leslie A: **Tissue-resident innate immunity in the lung.**
589 *Immunology* 2020, **159**:245-256.
- 590 56. Szabo PA, Miron M, Farber DL: **Location, location, location: Tissue resident memory T**
591 **cells in mice and humans.** *Sci Immunol* 2019, **4**.
- 592 57. Tay MZ, Poh CM, Renia L, MacAry PA, Ng LFP: **The trinity of COVID-19: immunity,**
593 **inflammation and intervention.** *Nat Rev Immunol* 2020, **20**:363-374.

595

596

597

598

599 **Figure legends**

600 **Fig. 1** Workflow of a data-driven study: from genetic factor to molecular phenotype.

601 The study has four major levels. Level 1: we collected the current largest COVID-19 genome-
602 wide association study (GWAS) datasets and a non-duplicated replicate of the severe COVID-19
603 GWAS dataset. Level 2: we utilized the cutting-edge statistical approaches (transcriptome-wide
604 association study and colocalization analysis) and public functional genomics annotations to
605 dissect the genetic effects on gene expression (Methods). Then, we cross-validated our findings
606 of these methods to ensure the robustness. Level 3: we adapted single cell RNA sequencing
607 dataset from COVID-19 bronchoalveolar lavage fluid samples. We applied differentially
608 expressed gene analysis and machine learning methods to characterize the molecular changes of
609 candidate gene at single cell level from COVID-19 moderate and severe patients. We conducted
610 extensive literature review to explain our observations. Level 4: we proposed a mechanism for
611 explaining the “causal” association of genetic factors and the severity of COVID-19 patients.

612

613 **Fig. 2** Manhattan plots illustrating the z scores of transcriptome-wide association study (TWAS)
614 genes.

615 TWAS z scores for two genome-wide association study (GWAS) datasets of susceptibility to
616 severe COVID-19 using lung and whole blood tissue models. The upper panel shows the results
617 from GWAS_{HGI} and the lower panel from GWAS_{SCGG} (see Methods). The round and triangle
618 points denote lung and whole blood tissues, respectively, in the TWAS analysis. Dashed
619 horizontal lines denote the Bonferroni-corrected significance threshold ($|z| = 4.56$, $p < 5 \times 10^{-6}$).
620 Significant genes were highlighted with their gene symbol.

621

622 **Fig. 3** Functional genomic annotation on *3p21.31* locus with signals from GWAS_{HGI}.

623 (a) LocusZoom view of the association signals of SNPs at the *3p21.31* locus of GWAS_{HGI}. The

624 x-axis is the chromosome position in million base pairs (Mb) on GRCh37 reference genome and

625 y-axis represents the $-\log_{10}$ (p-value) from GWAS_{HGI} dataset. The color indicates the strength of

626 linkage disequilibrium from the lead SNP rs35081325. The genes within the region are annotated

627 in the lower panel. A vertical blue line labels the position of the lead SNP rs35081325 to denote

628 the relationship of GWAS variants to other datasets: expression quantitative trait (eQTL) (Fig.

629 3b), chromatin interaction (Fig. 3c), and imputed Roadmap functional elements (Fig. 3d). (b)

630 The significant eQTLs associated with *CXCR6* expression in this region. The *cis*- eQTL datasets

631 include two whole blood datasets [Biobank-based Integrative Omics Studies (BIOS) QTL and

632 eQTLGen] and one T follicular helper cell dataset (DICE). The y axis represents the $-\log_{10}$ (p-

633 value) from the eQTL studies. (c) The significant Hi-C interactions in normal lung fibroblast cell

634 line (IMR90). Blue blocks denote the target and bait regions, and red arcs indicate the

635 interactions between functional elements. (d) The region annotated with the chromatin-state

636 segmentation track (ChromHMM) from the Roadmap Epigenomics data for T-cell and lung

637 tissue. The Roadmap Epigenomics cell line IDs are shown on the left side: E017 (IMR90 fetal

638 lung fibroblasts Cell Line), E033 (Primary T Cells from cord blood), E034 (Primary T Cells

639 from blood), E038 (Primary T help naïve cells from peripheral blood), E039 (Primary T helper

640 naïve cells from peripheral blood), E040 (Primary T helper memory cells from peripheral blood

641 1), E041 (Primary T helper cells PMA-Ionomycin stimulated), E042 (Primary T helper 17 cells

642 PMA-Ionomycin stimulated), E043 (Primary T helper cells from peripheral blood), E044

643 (Primary T regulatory cells from peripheral blood), E045 (Primary T cells effector/memory

644 enriched from peripheral blood), E047 (Primary T CD8 naïve cells from peripheral blood), E048

645 (Primary T CD8 memory cells from peripheral blood), E088 (Fetal lung), E096 (Lung), E114
646 (A549 EtOH 0.02pct Lung Carcinoma Cell Line), and E128 (NHLF Human Lung Fibroblast
647 Primary Cells). The colors denote chromatin states imputed by ChromHMM, with the color key
648 in the gray box (Methods).

649

650 **Fig. 4** Single cell transcriptome analysis of the severe and moderate COVID-19 patients.

651 **(a)** Relative expression of the lung resident memory CD8⁺ T (T_{RM}) signature genes in T_{RM} cells
652 and conventional CD8⁺ T cells in moderate patients. **(b)** Relative expression of the T_{RM} featured
653 genes in T_{RM} cells and conventional CD8⁺ T cells in severe patients. **(c)** *CXCR6* expression in the
654 T_{RM} cells of moderate and severe patients. We split the T_{RM} cells from the annotation of the
655 original paper with 31 marker genes (Methods). We conducted a two-sided non-parameter
656 Wilcoxon rank sum test to test whether *CXCR6* was differentially expressed in moderate (red)
657 and severe (blue) groups of T_{RM} cells. “***” indicates it is genome-wide significant after
658 multiple-test correction of all expressed genes. The small points denote the normalized
659 expression in each cell. Mean normalized expression of *CXCR6* in each group is highlighted with
660 the largest circle in black. **(d)** Pseudotime inference for the moderate and severe T_{RM} cells. The
661 red and blue points on t-Distributed Stochastic Neighbor Embedding (tSNE) projection denote
662 the T_{RM} cells from moderate and severe patients, respectively. The x-axis and y-axis are the first
663 and second dimension of the tSNE, respectively. **(e)** Relative expression of the *CXCR6* and naïve
664 and effector T cell markers along the pseudotime proportional to the green color. The gene
665 expressions are scaled by cells. Cells from moderate and severe groups are annotated in blue and
666 red. **(f)** Relevance score for hallmark pathways from the molecular signatures database
667 (MSigDB) along the pseudotime. The relevance score (R^2 coefficient of determination) indicates

668 the proportion of variance in the pseudotime explained by the genes in the hallmark pathways.

669 (g) Relevance score for transcription factors and their target genes along the pseudotime. The

670 relevance score denotes the proportion of variance in the pseudotime explained by the target

671 genes regulated by the transcription factor.

672

673 **Fig. 5** The proposed *CXCR6* regulation mechanism on COVID-19 severity.

674 We proposed one pathogenesis mechanism using current knowledge to explain how the lower

675 expression of *CXCR6* could be associated with the outcome of severe COVID-19 symptoms,

676 which was supported by our findings of the genetic factors on decreasing the *CXCR6* expression

677 and aligned with our observations from single cell transcriptome analysis. The star on the DNA

678 indicates the host genetic effects.

679

680 **Table 1:** Summary of TWAS and colocalization analyses in tissues and cell lines.

Gene symbol	Tissue	Discovery: GWAS _{HGI}				Validation: GWAS _{SCGG}			
		TWAS z	TWAS p	PP	colocalized SNP p	TWAS z	TWAS p	PP	colocalized SNP p
<i>CXCR6</i>	Lung	-8.53	1.57×10 ⁻¹⁷	0.79*	rs34068335 5.02×10 ⁻²²	-4.19	2.84×10 ⁻⁵	ns	-
	T follicular helper cells	-	-	0.99**	rs35081325 3.82×10 ⁻³⁹	-	-	0.99**	rs35081325 2.49×10 ⁻¹⁰
<i>CCR9</i>	Whole blood	6.50	7.90×10 ⁻¹¹	ns	-	6.26	3.78×10 ⁻¹⁰	ns	-

681 GWAS_{HGI} denotes the GWAS dataset from the Host Genetics Initiative.

682 GWAS_{SCGG} represents the GWAS dataset from the Severe COVID-19 GWAS Group.

683 PP: posterior probability.

684 z: z score.

685 p: p-value.

686 *: statistically significant by the colocalization posterior probability (CLPP) from eCAVIAR.

687 **: statistically significant by the regional colocalization probability (RCP) from fastENLOC.

688 ns: no significant colocalization from either eCAVIAR or fastENLOC.

689 -: no available data.

690

691 **Table 2:** Counts and ratio of T_{RM} cells in moderate and severe patients.

Patient group (sample size)	# CD8 ⁺ T cells	# T _{RM} cells	T _{RM} cell proportion ratio (Moderate/Severe)
Moderate (3)	2,135	675	3.32
Severe (6)	4,356	415	

692 #: the counted number.

693 T_{RM} cells: the resident memory CD8⁺ T cells as defined in Methods.

694

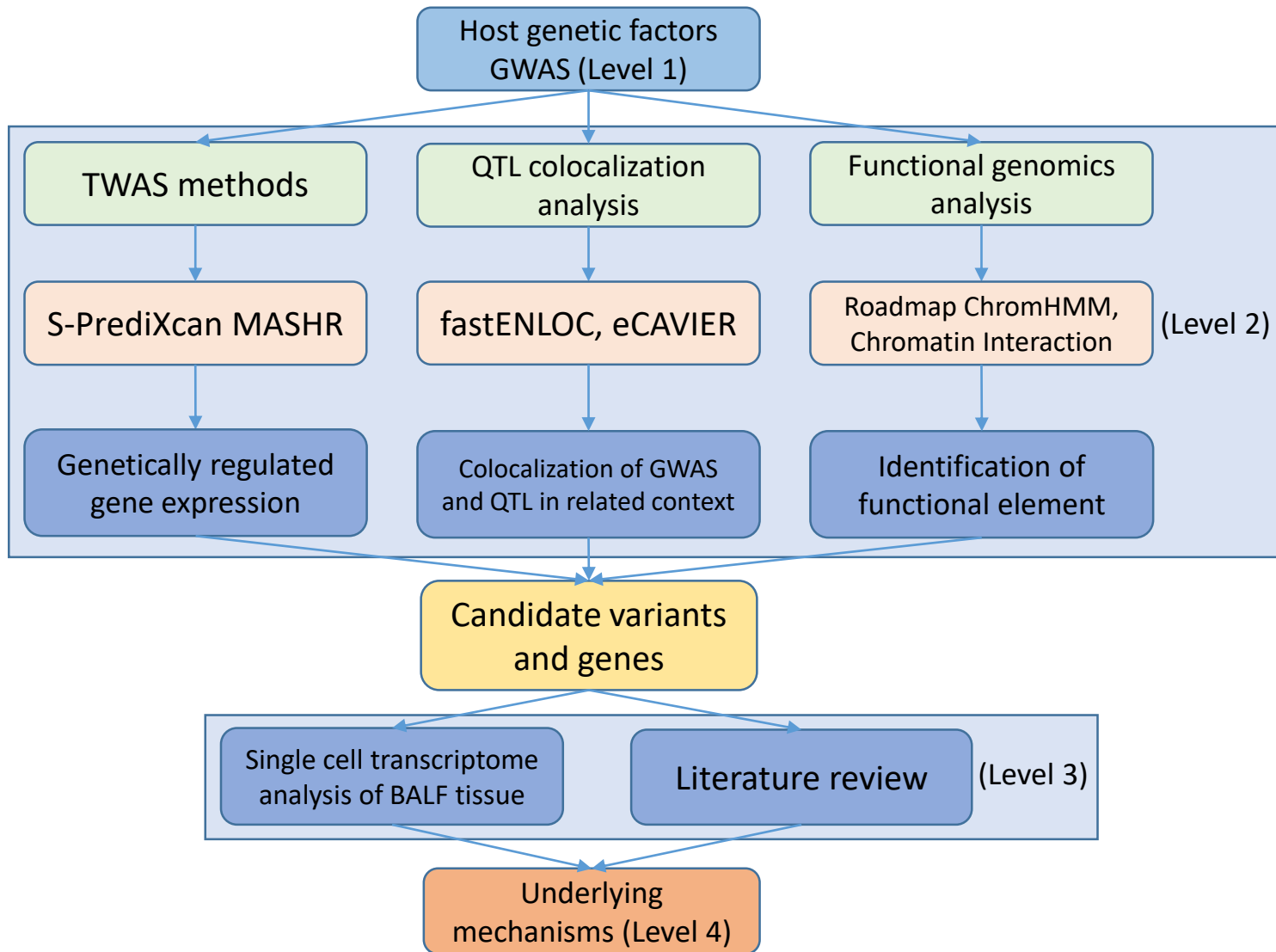
695

696 **Additional files**

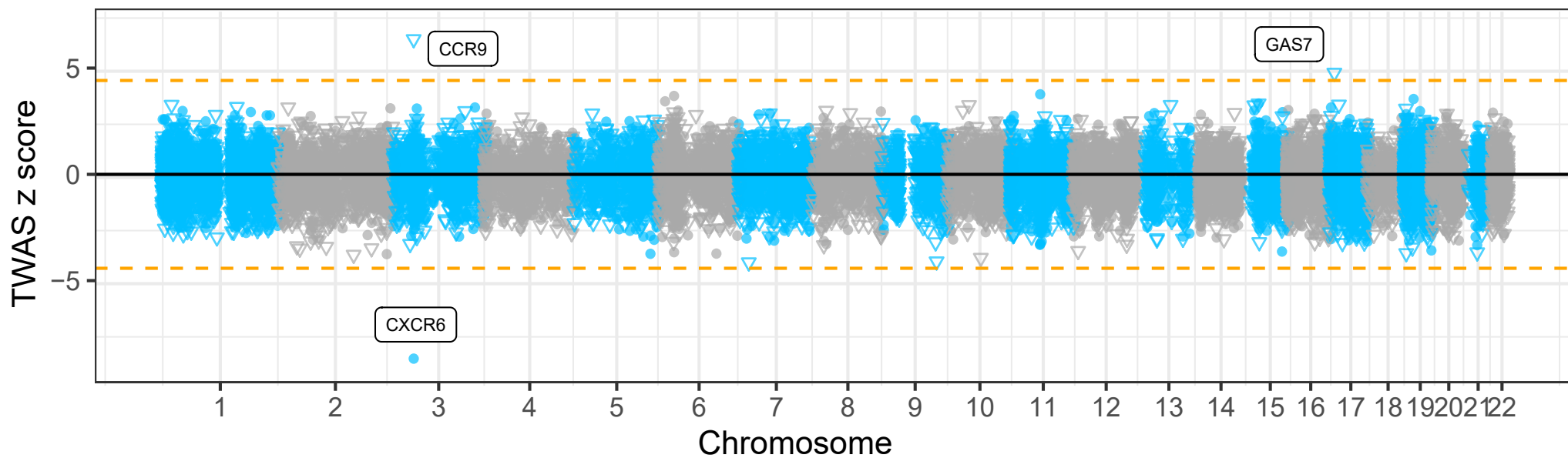
697 Additional file 1.pdf: Fig S1: Sequence logos representing DNA binding site generated from
698 position weight matrix (PWM) for transcription factor RELA and SP1. Fig. S2. Violin plots
699 showing the distribution of key features between moderate and severe patients. Fig. S3.
700 LocusZoom views for two Host Genetics Initiates GWAS datasets at *3p21.31* locus. Table S1:
701 Hallmark pathways and their relevance scores. Table S2: Transcription factors and their
702 relevance scores.

703

704 Additional file 2.xls: Table S3: Predicted transcription factors (SP1 and RELA) bind affinity
705 alterations on genome-wide significant SNPs at locus *3p21.31*.

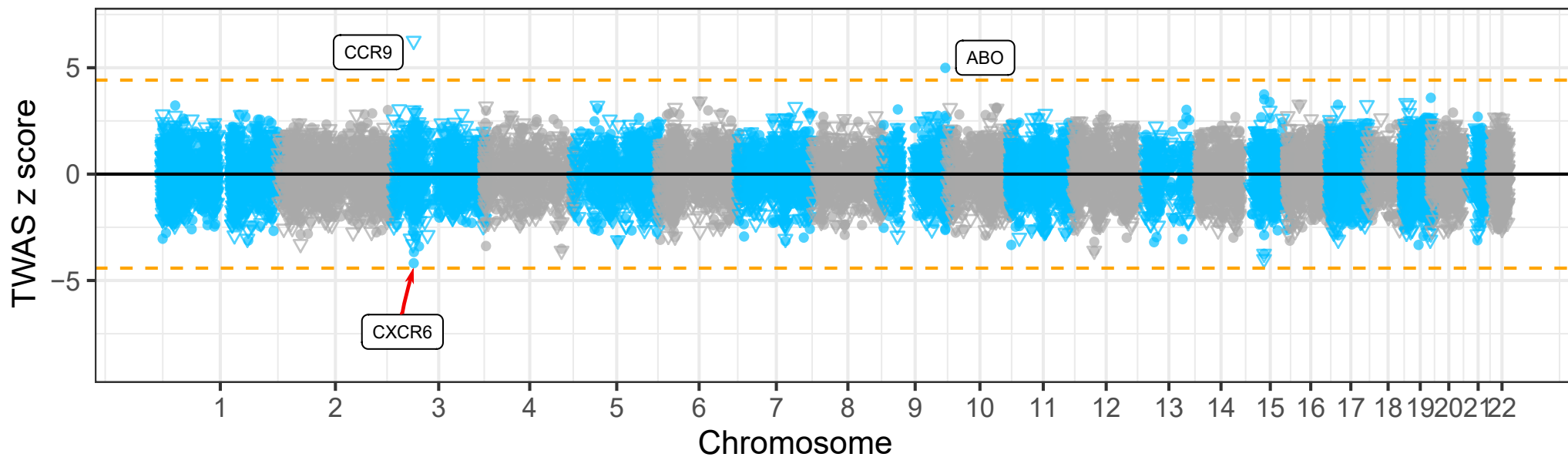


GWAS_{HGI}

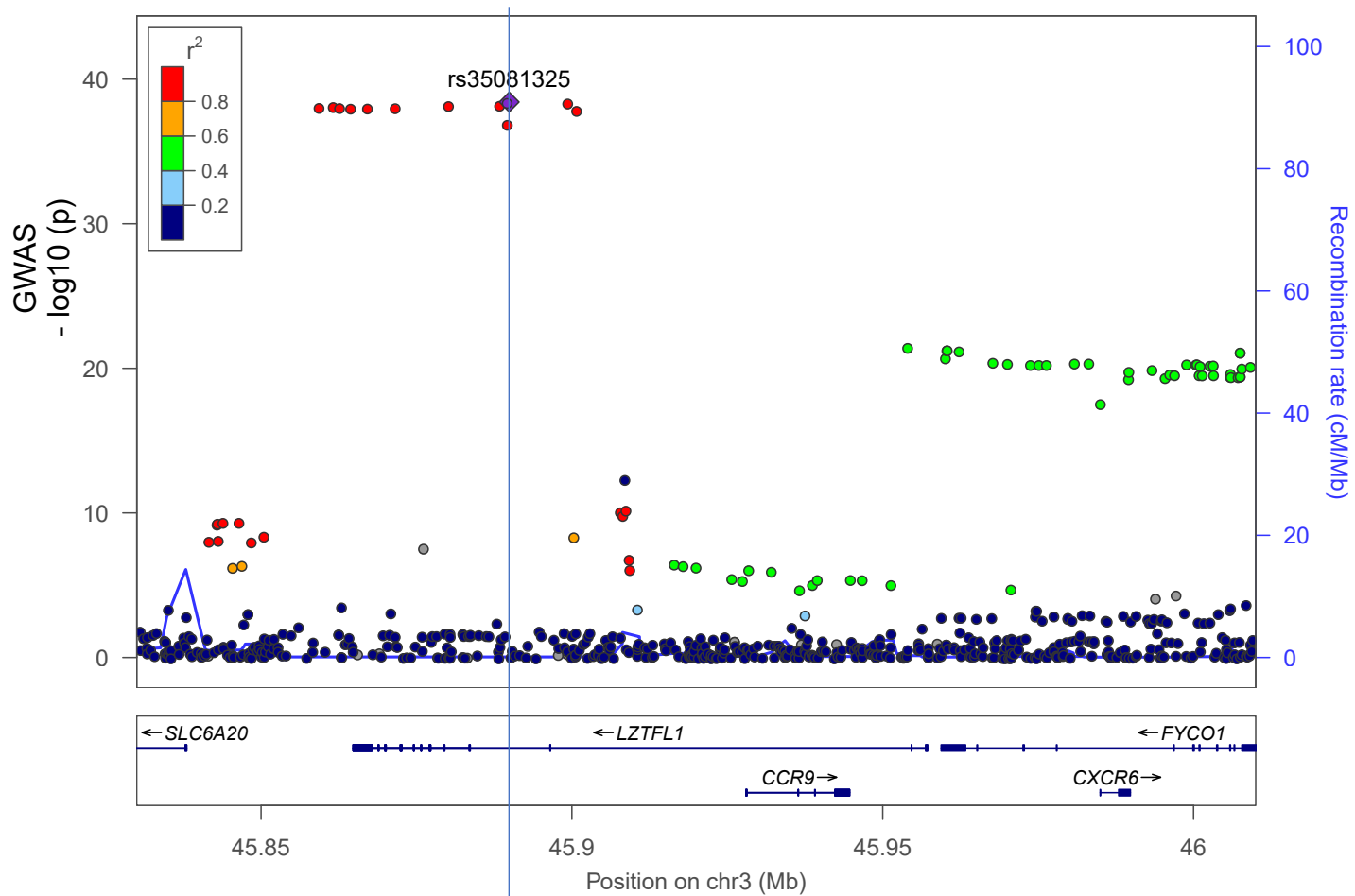


● Lung ▽ Whole Blood

GWAS_{SCGG}



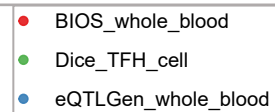
A



B

IMR90
Hi-C

CXCR6 eQTL
-log₁₀(p)

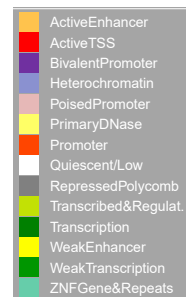


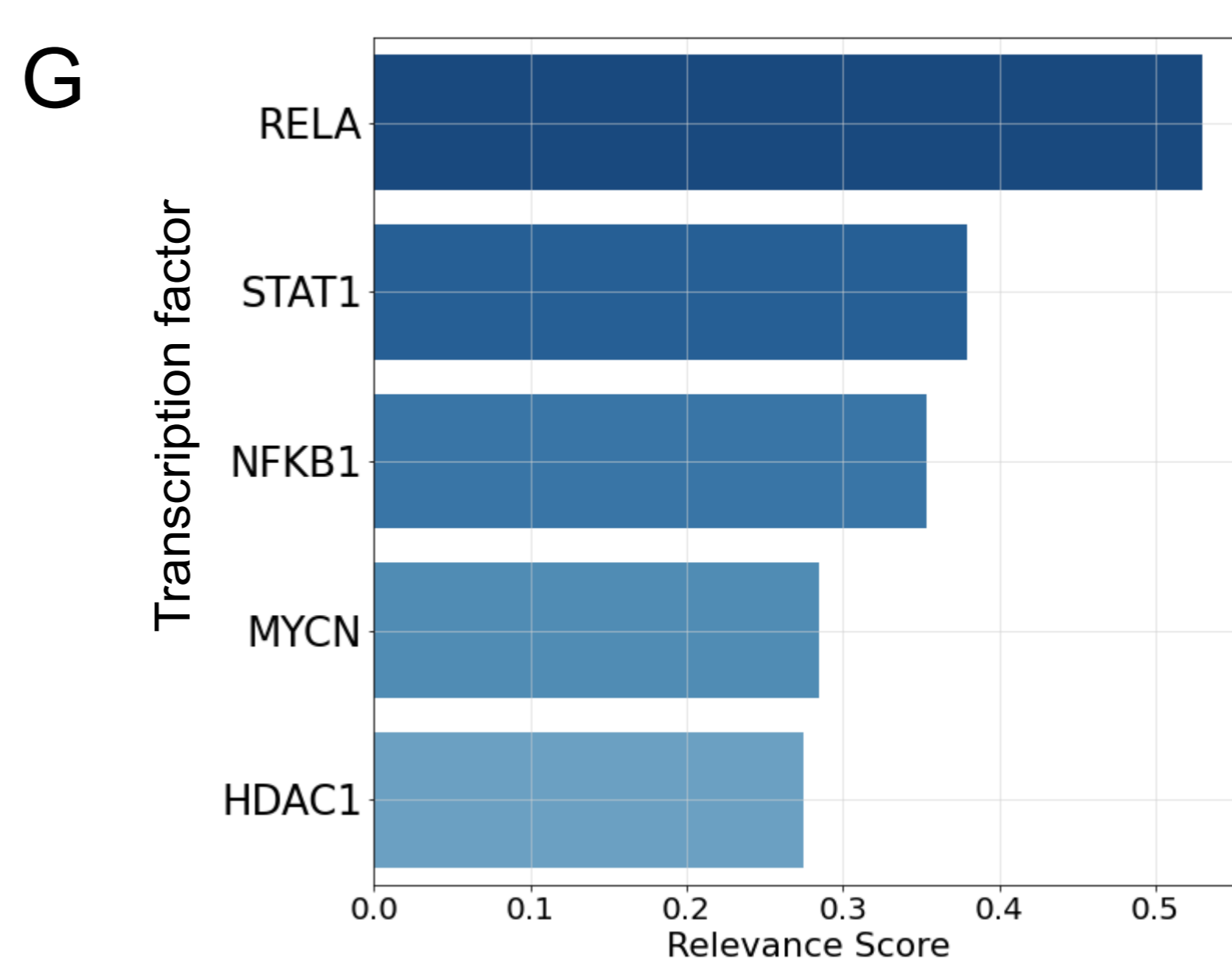
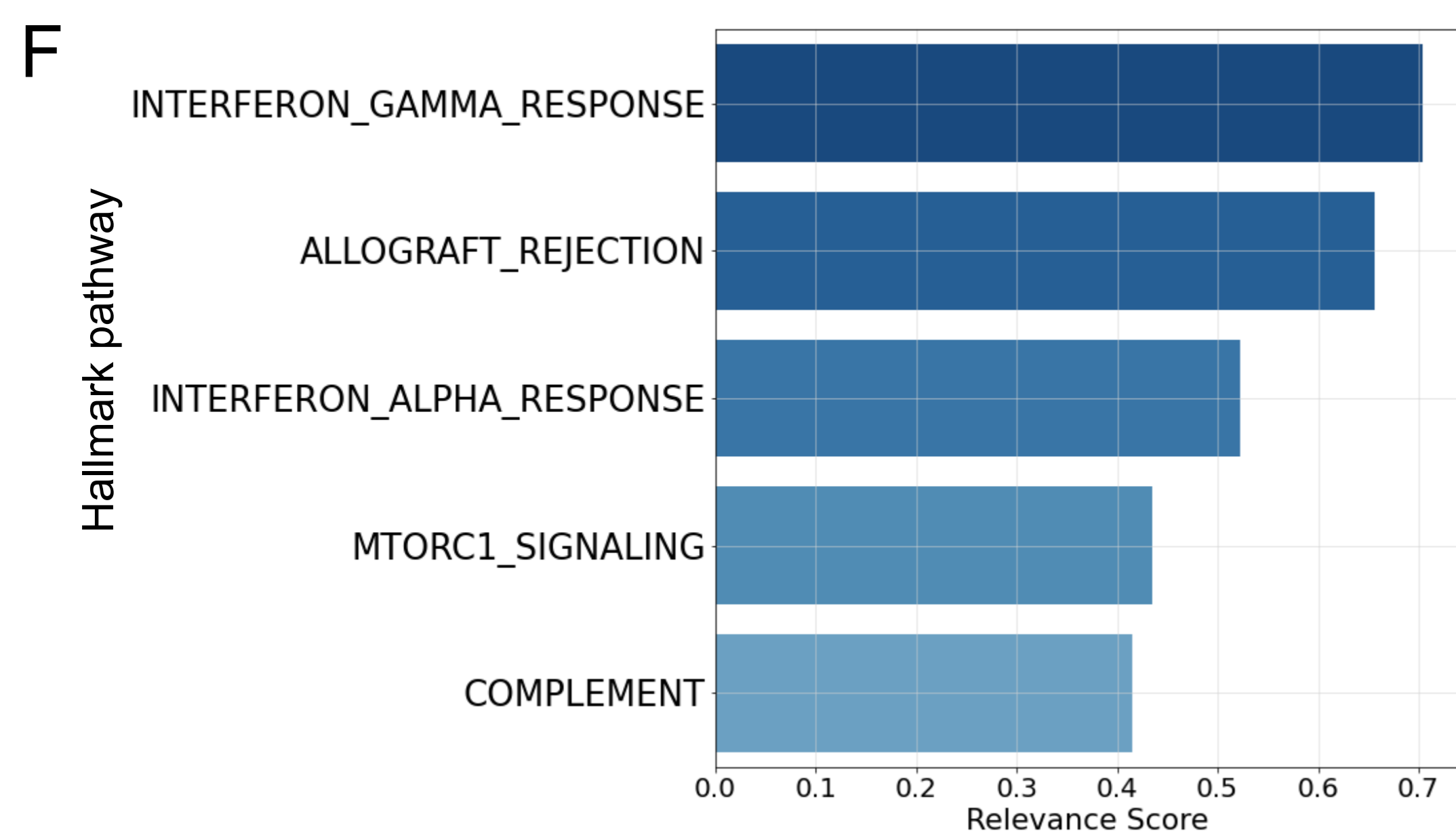
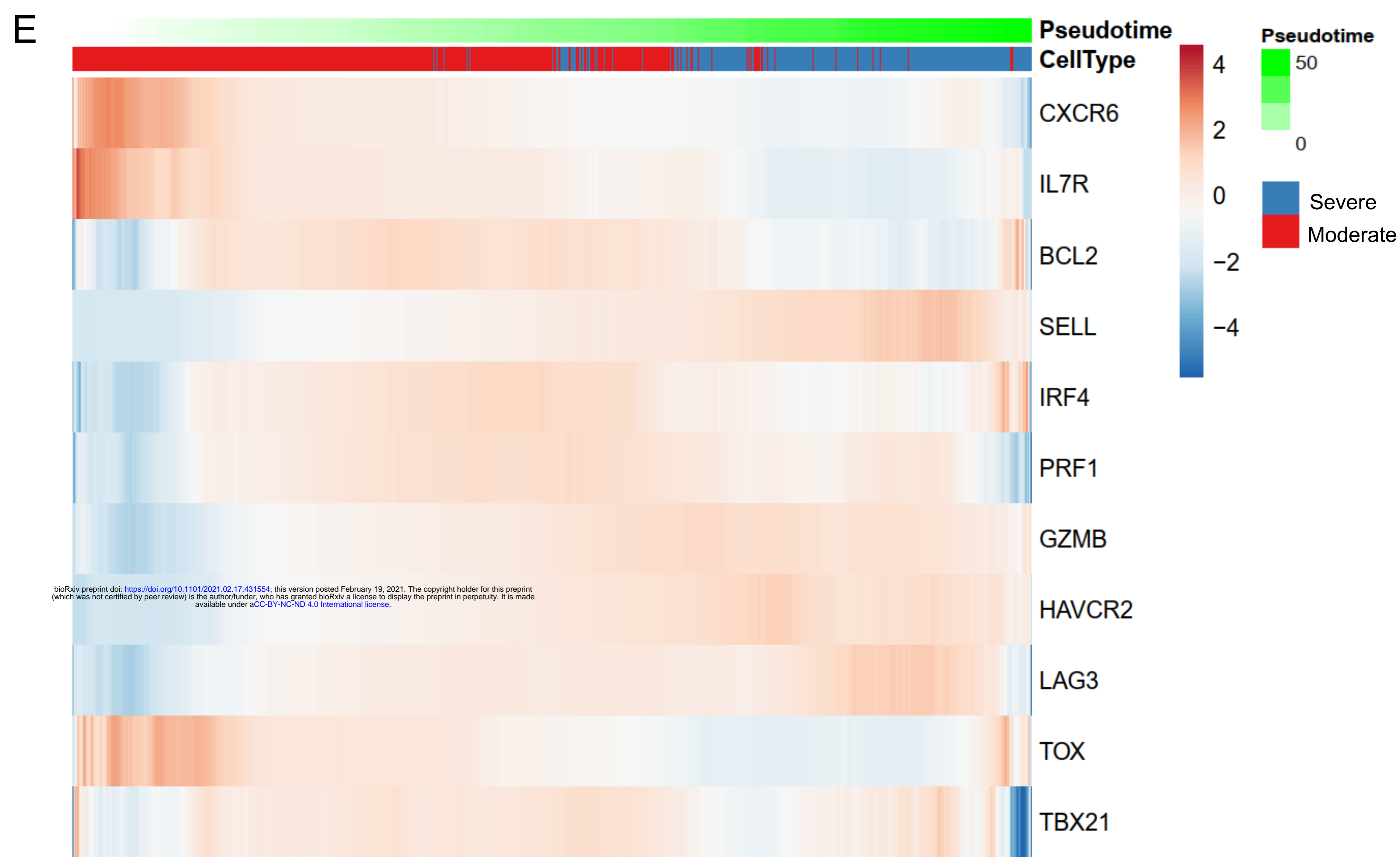
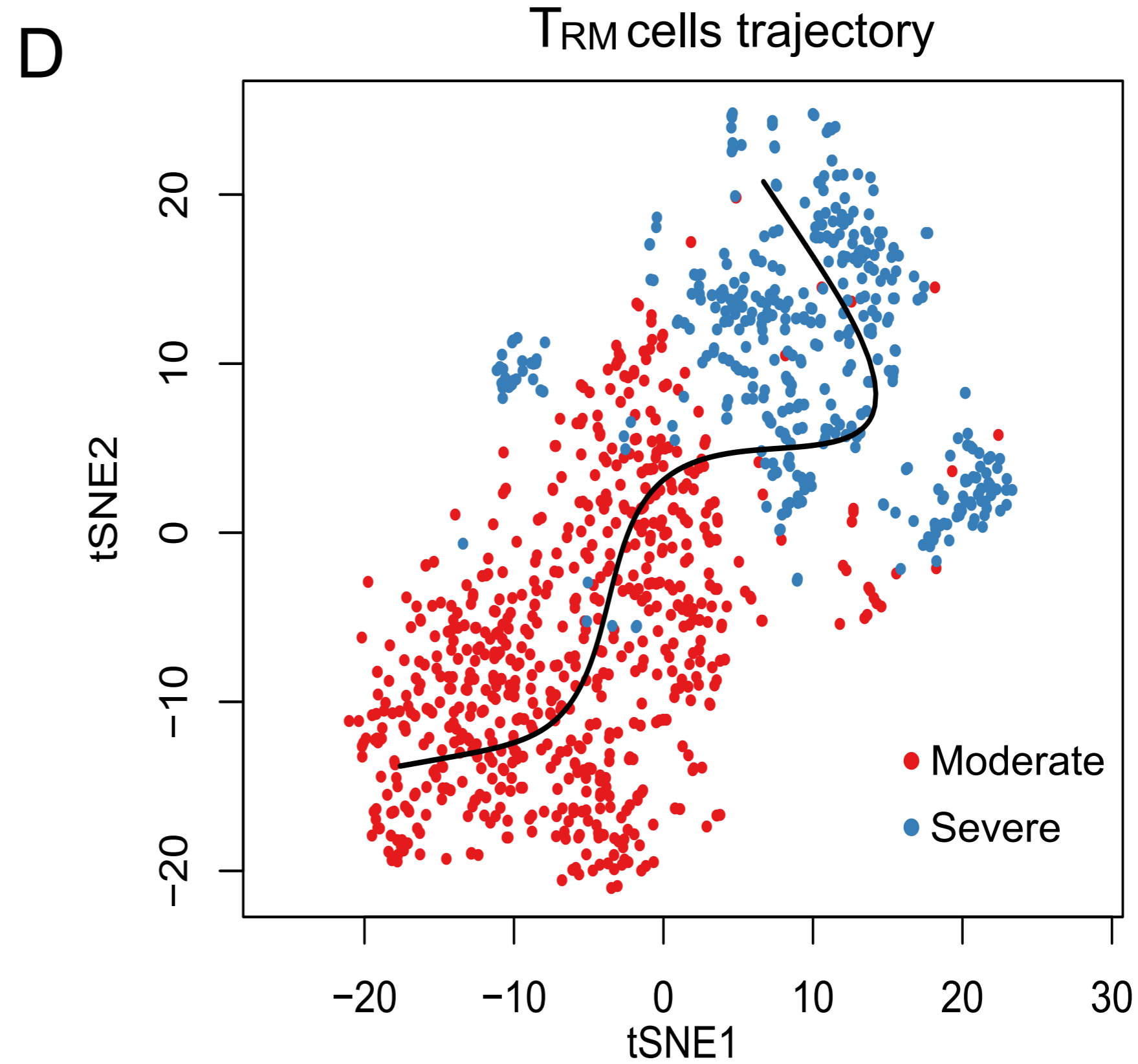
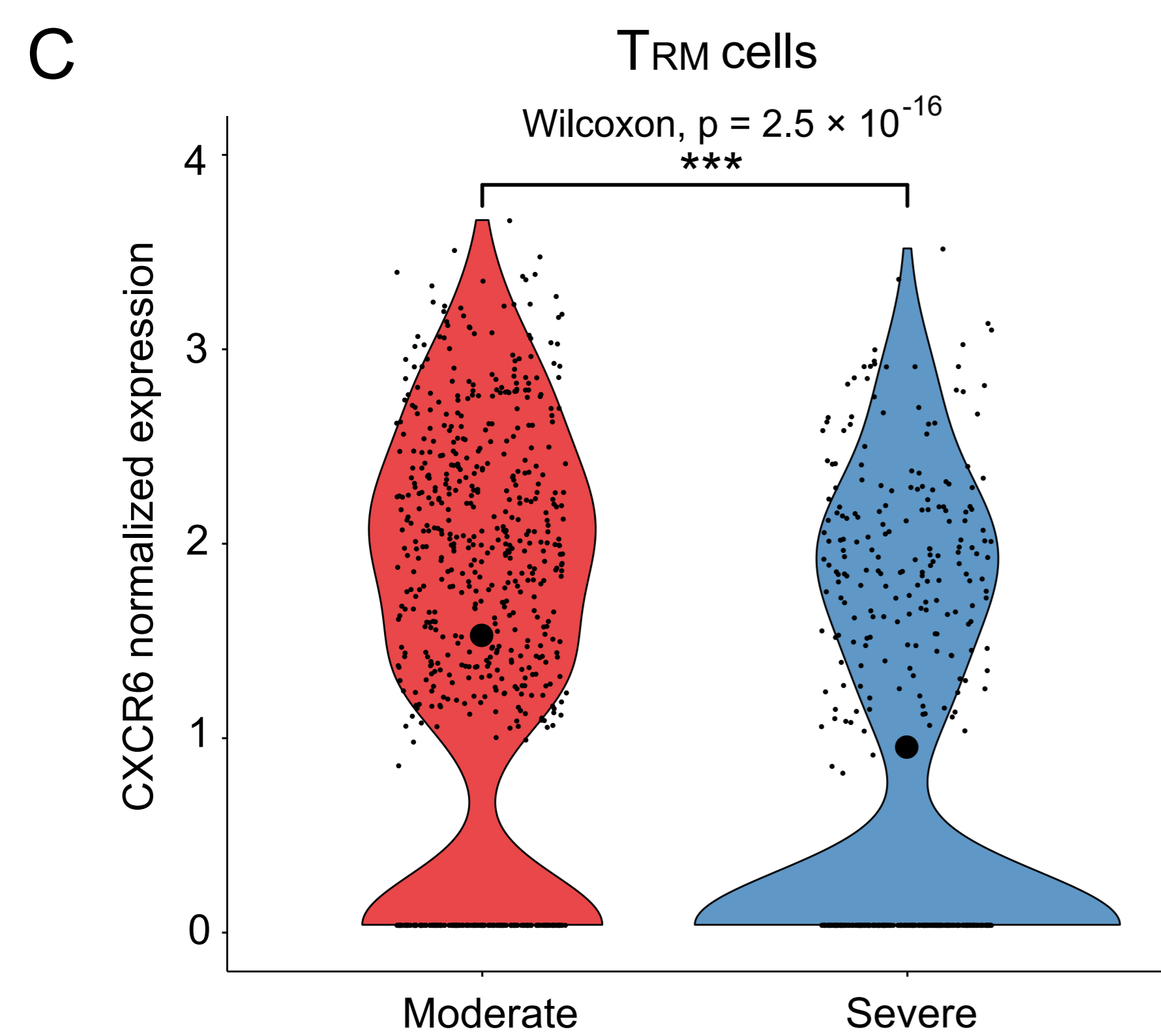
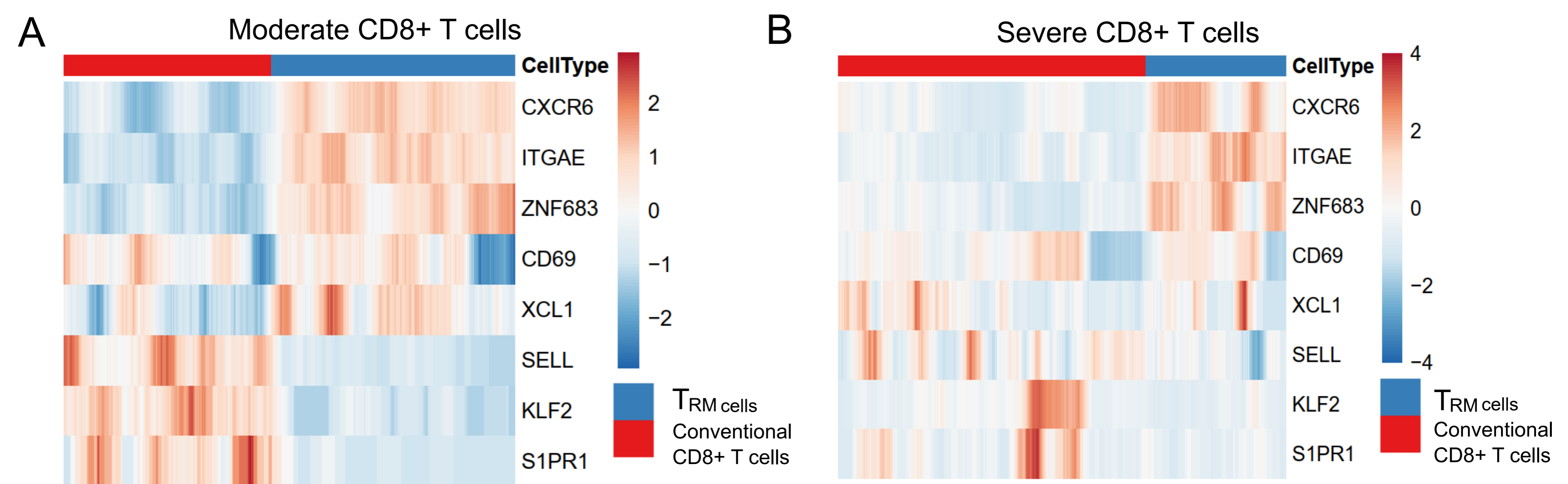
C

IMR90
Hi-C

D

Roadmap
chromatin
state

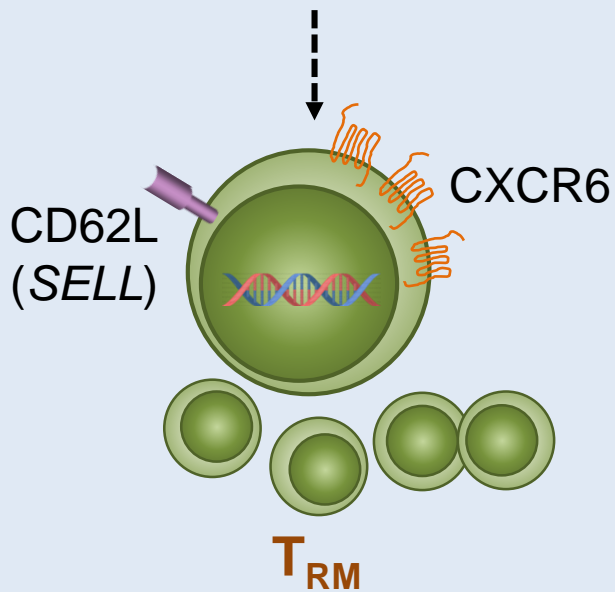




Moderate COVID-19



cis-regulator of CXCR6

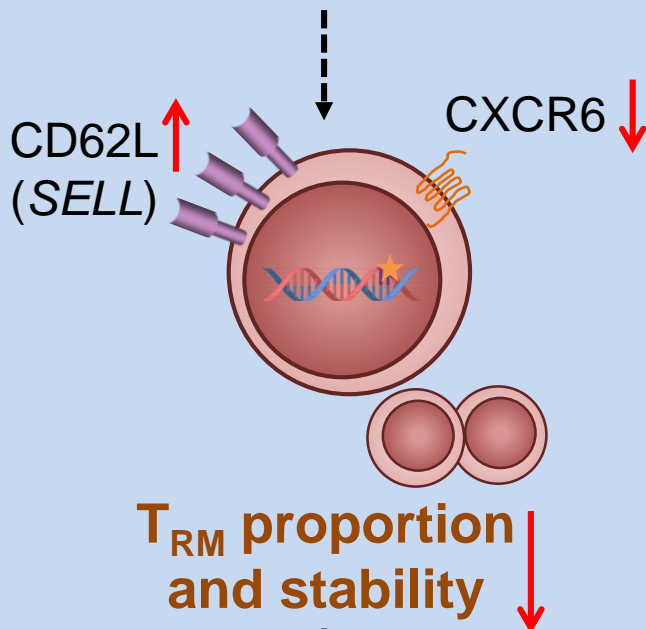


Viral clearance
Resolving inflammation

Severe COVID-19



Host genetic variations



Viral replication
Tissue damage